Preferred Orientation of a Physisorbed Molecular Catalyst and Implications for Selectivity

Guillaume P Laurent, Samuel L Leonard, Mita Halder, Damien B Culver, Peng Xu, Mark S Gordon, Frédéric A Perras

ACS PHYSICAL CHEMISTRY Au
AN OPEN ACCESS JOURNAL OF THE AMERICAN CHEMICAL SOCIETY

pubs.acs.org/physchemau
Article

Preferred Orientation of a Physisorbed Molecular Catalyst and Implications for Selectivity

Guillaume P. Laurent, Samuel L. Leonard, Mita Halder, Damien B. Culver, Peng Xu, Mark S. Gordon, and Frédéric A. Perras*

Cite This: ACS Phys. Chem Au 2025, 5, 293−301
Read Online
ACCESS | Metrics & More | Article Recommendations | Supporting Information

ABSTRACT: Confinement effects in stereoselective catalysis have been the topic of prolonged inquiry. Results have been largely mixed, with confinement having been reported to both enhance and degrade selectivity. Our ability to understand the surface's impact on catalytic mechanisms, and thus selectivity, has been severely hindered by the low level of details commonly seen in the structures of supported metal complexes. Recent developments in sensitivity-enhanced NMR are revealing not only the molecular structure of surface sites but also their configuration, orientation, and proximities to neighboring molecules. In studying [Rh(cyclooctadiene)((*S*)-(−)-2-aminomethyl-1-ethyl-pyrrolidine)]-CF_3SO_3 noncovalently immobilized to silica, an enantioselective hydrogenation catalyst, we observed a strong preference for a particular orientation of the complex relative to the support surface. We discuss how preferential adsorption may help reduce the number of competing reaction pathways and, in turn, have outsized effects on selectivity.

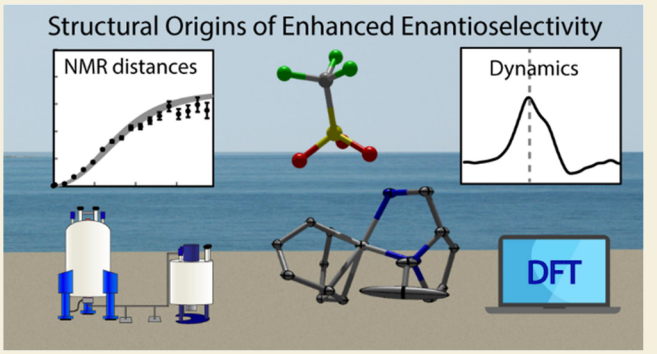

KEYWORDS: *heterogeneous catalysis, dynamic nuclear polarization, solid-state NMR, asymmetric catalysis, dipolar coupling*

1. INTRODUCTION

There has been considerable interest in utilizing confinement or surface effects in heterogeneous catalysis to enhance selectivity.[1−4] Probably the most well-known, and economically significant, examples are Ziegler−Natta catalysts that are able to produce polyolefins with higher molecular weights and stereoselectivities than early homogeneous counterparts, presumably due to steric interactions between the polymer and the catalyst surface preventing conformational rearrangements.[5−8] Marks and co-workers reported that Cp*$ZrMe_3$ chemisorbed to sulfated alumina produces isotactic polyolefins due to complex orientation and support steric effects on the growing polymer chain.[9] Gauvin and co-workers have also shown that nonselective lanthanide-based olefin polymerization catalysts become stereoselective when supported onto silica.[10,11] In large part, however, our understanding of these effects is severely lacking, and the designation of the support primarily as a steric force may, in most other cases that do not involve macromolecule synthesis, be an oversimplification.

This is perhaps best exemplified by one of the earliest examples of heterogeneous single-site enantioselective catalysis wherein Cu bis(oxazoline) complexes were immobilized noncovalently onto laponite, a synthetic clay, and used as cyclopropanation catalysts.[12] The immobilization led not to an increase in selectivity but rather a reversal in the enantioselectivity. The effect was not observed when using graphite or silica as a support, indicating that the primary changes in selectivity were due to substrate interactions with the charged clay surface.[13,14] The effects of secondary interactions from silanol groups on silica surfaces have also been reported in some cases to promote a higher enantioselectivity and in others to have detrimental effects.[15−17]

There is no general trend that summarizes confinement effects in stereoselective catalysis. Of course, the most well-known examples are those where selectivity is increased as a result of confinement or heterogenization,[18−32] but there are numerous examples where the opposite has been observed.[12,33−40] To better understand spatiochemical effects in enantioselective heterogeneous catalysis, Thomas, Raja, and others studied enantioselective Rh-catalyzed hydrogenation reactions as a function of the support pore size.[1] Most effective was the use of a noncovalently immobilized complex presumed to interact with the surface through hydrogen bonding interactions (Figure 1).[32] Such a structure in principle allowed

Received: January 21, 2025
Revised: February 25, 2025
Accepted: February 26, 2025
Published: March 7, 2025

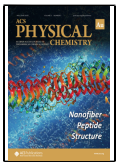

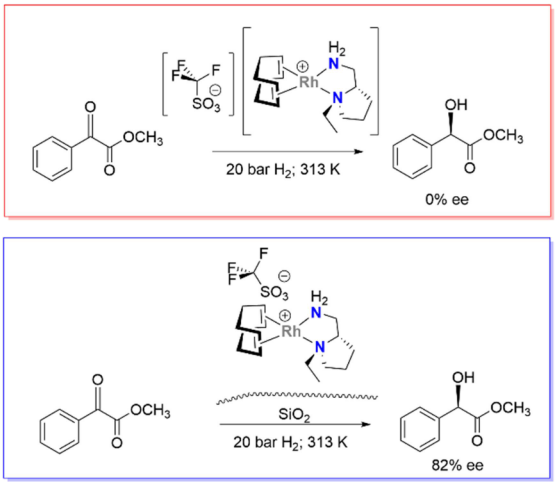

Figure 1. $[Rh(cod)(aep)]CF_3SO_3$ catalyzes the asymmetric hydrogenation of methyl benzoylformate.[32] Enantiomeric excess (ee) is dramatically increased when the complex is physisorbed onto mesoporous silica.

the decoupling of chemical and steric effects. They observed a dramatic increase in enantioselectivity from heterogenization, and a selectivity that increased with decreasing pore size.

Recent developments in solid-state nuclear magnetic resonance (NMR) spectroscopy and its application to the structural characterization of single-site catalysts have the potential to yield transformative new insights into stereoselective catalysis by revealing the nature of the interactions between the catalyst and the support, in addition to the overall three-dimensional geometry of the site. Sensitivity enhancements from dynamic nuclear polarization (DNP)[41−43] have enabled the measurement of accurate interatomic, and atom-to-surface distances and revealed the first three-dimensional structures of surface sites.[44−52] Similarly, the possibility to probe intersite distributions using DNP-enhanced NMR and fast-magic-angle spinning (MAS)[53−56] and measure intersite distances has been demonstrated.[57−59] Herein we apply solid-state NMR to study the structure of [Rh(cyclooctadiene)((*S*)-(−)-2-aminomethyl-1-ethyl-pyrrolidine)]CF_3SO_3 ([Rh(cod)-(aep)]CF_3SO_3) supported on mesoporous silica. This complex was found to adopt a strongly preferred orientation on the support, despite the noncovalent nature of the complex-surface interaction, a fact which may explain the supported complex's higher selectivity in asymmetric hydrogenation.[32]

2. EXPERIMENTAL SECTION

2.1. Synthesis

All procedures were performed using standard Schlenk or glovebox techniques under an atmosphere of nitrogen or argon. Pentane, methylene chloride, diethyl ether, and tetrahydrofuran were degassed by sparging with nitrogen, dried by filtering through activated alumina columns, and stored under nitrogen.

2.1.1. [Rh(cod)(aep)]CF_3SO_3. $[Rh(cod)(aep)]CF_3SO_3$ was prepared using modified literature procedures.[32] 99.5 mg (0.20 mmol) of $[RhCl(cod)]_2$ was dissolved in 10 mL of THF to which was added 103.5 mg (0.40 mmol) of AgO_3SCF_3. The mixture was then stirred for 1 h. The AgCl precipitate was allowed to settle for 1 h, after which the solution was collected by decantation. 90 μL (0.65 mmol) of (*S*)-(−)-2-aminomethyl-1-ethylpyrrolidine was then added to the above solution, which was stirred for an additional hour. The solution was subsequently concentrated in vacuo to half its original volume and pentane was added to precipitate $[Rh(cod)(aep)]CF_3SO_3$, which was collected through decanting and washed with pentane (2 × 10 mL) and diethyl ether (2 × 10 mL). The resulting powder was then dried in vacuo for 45 min and stored in an Ar filled glovebox. Yield = 158 mg (81%). Solution phase ^{1}H, ^{13}C, and ^{19}F NMR spectra (Figures S1−S3) agree with prior literature report, however, the assignments have been updated in the ESI.[32]

2.1.2. [Rh(cod)(aep)]CF_3SO_3/SiO_2 (Modified from Ref 32). Mesoporous silica supports (Davisil 923, 636, 646, and ^{29}Si-enriched MCM-41[51]) were dried for 9 h at 550 °C under dynamic vacuum using a tube furnace. The resulting dry supports were stored in an Ar glovebox. 33 mg (68 μmol) of $[Rh(cod)(aep)]CF_3SO_3$ was dissolved in 15 mL of CH_2Cl_2 to which was added 130 mg of silica. The mixture was then stirred overnight, and the supernatant was decanted from the solids. The solids were then washed with CH_2Cl_2 (4x 5 mL) and dried for 6 h in vacuo.

The Rh loading for the MCM-41-supported sample was measured to be 0.230 mmol/g (2.37 wt %) using ICP-MS. Diffuse reflectance infrared Fourier transform infrared (DRIFTS) spectra were measured on a Bruker ALPHA II spectrometer contained within an argon-filled glovebox and spectra were recorded within the 4000−400 cm^{-1} range. Samples were prepared by adding a thin layer of sample on a flat bed of dry KBr (dried at 180 °C under high vacuum and stored in an argon filled glovebox).

2.2. Solid-State Nuclear Magnetic Resonance

^{1}H NMR chemical shift anisotropy (CSA) recoupling experiments were performed using a phase-sensitive $R20_9^8(270_090_{180})$ symmetry-based CSA recoupling experiment[60] at room temperature on a Bruker AVANCE NEO 600 MHz NMR spectrometer equipped with a 1.3 mm PhoenixNMR MAS probe. The MAS frequency was set to 50 kHz. A 324 μs phase-shifted recoupling block was used to generate the phase difference required for States processing. The t_1 evolution period was incremented in 108 μs increments and a total of 64 increments were acquired, each consisting of 32 scans. Data were processed as described in ref 60. The recycle delay was set to 4.3 s for the dry silica-supported sample, and 2.6 s otherwise.

^{1}H{^{19}F} symmetry-based rotation-echo double-resonance (S-REDOR) experiments[61,62] were performed at room temperature using an Agilent DD2 400 MHz NMR spectrometer equipped with a Varian HFXY quadruple-resonance 3.2 mm MAS probe. The MAS frequency was set to 20 kHz and the $SR4_1^2$ recoupling sequence[63] was applied to the ^{1}H nuclei for heteronuclear dipolar recoupling. The recycle delay was set to 2.6 s and a total of 128 scans were acquired for each spectrum. The recoupling time was incremented in 100 μs increments.

Fast-MAS ^{19}F NMR spectra were acquired at room temperature using a Bruker AVANCE III 600 MHz NMR spectrometer equipped with a 1.6 mm Varian fast-MAS probe. Samples were spun at 40 kHz and spectra were acquired using a rotor-synchronized Hahn echo sequence. The radiofrequency power was set to 62.5 kHz and the recycle delay was equal to 1 s.

^{13}C{^{29}Si} REDOR experiments[61] were performed at 100 K using a Bruker AVANCE III 400 MHz MAS-DNP spectrometer equipped with a 3.2 mm low-temperature triple-resonance MAS probe. Samples were impregnated with a 16 mM TEKPol[64] solution in dry deuterated[65] 1,1,2,2-tetrachloroethane (TCE-d2)[66] in a glovebox before being transferred to the 100 K precooled NMR probe. Hyperpolarized ^{1}H magnetization was transferred to ^{13}C nuclei using a 2 ms cross-polarization (CP) contact time. Radiofrequency powers for all other ^{29}Si and ^{13}C pulses equaled 50 kHz. MAS rates were set to 10 kHz and the recycle delays equaled 2 s. 1024 scans were accumulated for each recoupling time increment of 1.2 ms.

All multispin REDOR and S-REDOR data were analyzed using the INTERFACES program.[52] The data and input files are given in Section 2 of the Supporting Information.

2.3. Quantum Chemistry

Density functional theory (DFT) calculations were performed to probe the preferential adsorption of the [Rh(cod)(aep)] cation *in silico*. Calculations made use of a thin, partially dehydroxylated silica model from Ugliengo and co-workers.[67,68] onto which were placed

https://doi.org/10.1021/acsphyschemau.5c00007
ACS Phys. Chem Au 2025, 5, 293−301

[Rh(cod)(aep)] cations in particular orientations. Geometry optimizations were performed while maintaining the silicon hydride positions that terminate the bottom layer of the slab fixed, in addition to the unit cell dimensions. Calculations were performed using Quantum Espresso[69] using ultrasoft pseudopotentials, the PBE functional,[70] Grimme's D3 dispersion correction,[71] and a 40 Ry kinetic energy cutoff.

The resolution-of-the-identity (RI) second-order Møller-Plesset second-order perturbation theory (RI-MP2)[72] calculations were performed on truncated models of the above-mentioned plane-wave DFT-optimized structures to assess the importance of correlation in the relative adsorption energies. The models included all surface atoms in proximity to the complex and were truncated by hydrogens. All hydrogen atoms were optimized at the PBE-D3/TZ2P level of theory using the Amsterdam Density Functional program (see Supporting Information for coordinates),[73] and single-point RI-MP2MCPTZP/aug-cc-pVTZ-DK calculations were performed on the resulting geometries using GAMESS.[74−76]

3. RESULTS

3.1. Grafting Chemistry

DRIFTS spectroscopy (Figure 2) was applied to determine the adsorption chemistry when $[Rh(cod)(aep)]CF_3SO_3$ is immobilized onto silica. In addition to the observation of new stretching peaks from the ligands in $[Rh(cod)(aep)]CF_3SO_3$, we observed the decrease in intensity of the isolated silanol stretching peak and the appearance of a broad signal at approximately 3400 cm^{-1} after immobilization. Unlike what is observed with catalysts that graft via protonolysis reactions, we did not observe the consumption of the silanols suggesting that the complex is simply physisorbed. This is supported by the appearance of the broad signal common to hydrogen bonding interactions that is absent in the FTIR spectrum of the molecular precursor.

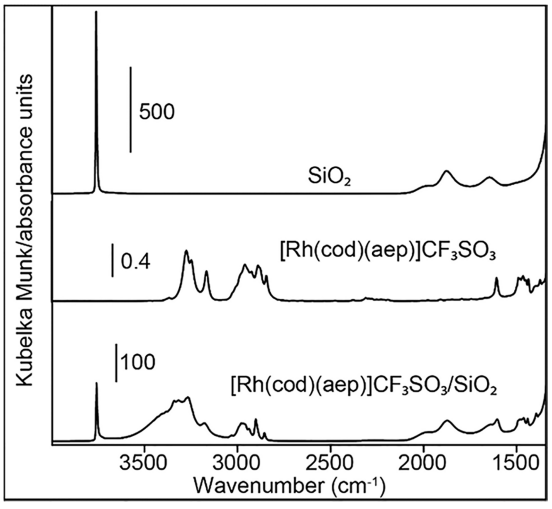

Figure 2. DRIFTS spectra of SiO_2 and $[Rh(cod)(aep)]CF_3SO_3/SiO_2$, and absorbance FTIR spectrum of $[Rh(cod)(aep)]CF_3SO_3$. The OH stretching peak is broadened and red-shifted by hydrogen bonding interactions in $[Rh(cod)(aep)]CF_3SO_3/SiO_2$.

3.2. Preferred Orientation

Given the physisorbed nature of the immobilized complex, it can theoretically adopt many orientations on the surface. Because surface silanols, and reactant-surface interactions, have been implicated in heterogeneous enantioselective catalysis,[13−17] measuring the preferential orientation of the complex at the surface may have significant impacts on selectivity. We performed ligand-surface distance measurements using ^{13}C-$\{^{29}Si\}$ REDOR experiments[51] to probe the complex's orientation and fitted the obtained data to a single orientation of the [Rh(cod)(aep)] cation on the surface (Figure 3). The structure search and fitting were accomplished using the open-source INTERFACES program.[52]

The search for the best fitting surface structure revealed a strong preference for the cation adopting an orientation with its NH_2 moiety facing away from the support. The structure in Figure 3c, for instance, represents the best-fit structure describing the gray-shaded fitting regions in Figure 3b and corresponds to a fit quality with a confidence interval of 99%.

We performed a second fitting attempt whereby the orientation of the complex was forced to adopt an opposite orientation, while still minimizing the difference between the experimental and computed REDOR data sets (see Supporting Information for details and input files). The best fit structure in this case is shown in Figure 3d, with the fits depicted as red shaded regions in Figure 3b. This orientation leads to the overestimation of the dephasing calculated for carbon E on the ligand (see Figure 3a for labels) and the simultaneous underestimation of the dephasing for carbons A, B, F, G and H. As shown in Figure 3e, linear combinations of the two best-fit orientations do not lead to an improvement of the fit quality, suggesting a strong preference for the orientation with the NH_2 moiety pointing away from the surface. Plotted is the total root mean squared deviation (RMSD) between calculated and computed REDOR dephasing curves with the populations of the two species being incremented in steps of 5%. Note that the change in slope in Figure 3e when the population of the opposite conformer is >40% is caused by the slightly overestimated dephasing for site G in the best-fit orientation.

To determine whether there is a strong energetic reason for the complex adopting this orientation we performed plane-wave DFT calculations to calculate the absorption energies for the two possible orientations of the complex. Calculations were replicated at two different locations on the surface (see coordinates in the Supporting Information and Figure S6) to probe a larger chemical space. The unit cell is capable of holding two [Rh(cod)(aep)] cations, and each model was designed such that the Rh complex was situated on either half of the unit cell. As such, we expect the calculations to largely explore the entire silica model surface.

For the two models based on the orientation depicted in Figure 3c, the complex was found to optimize to Rh−Si layer distances of 4.5 and 5.4 Å with surface plane−N−N vector angles of 70.1 and 67.8°. These DFT-optimized values were quite close to the mean values determined experimentally, namely 5.0 Å and 63.8°, implying that the experimentally measured conformation is indeed chemically sensible. Importantly, this rules out an earlier proposed model wherein the triflate anion would act as a linker, connecting the complex to the support through hydrogen-bonding interactions.[32]

The calculated adsorption energies for the models based on the orientation from Figure 3d, however, were 4.9 and 31.6 kJ/mol lower, in disagreement with experiment (Table S1). If a fully dehydroxylated quartz surface is used instead of a partially dehydroxylated amorphous silica model, the difference between the models in Figure 3c,d is reduced to 0.11 kJ/mol (Table S2, Figure S6), suggesting that electrostatic interactions between hydroxyls and the NH_2 moiety are responsible for the calculated differences in the amorphous models. Because DFT

https://doi.org/10.1021/acsphyschemau.5c00007
ACS Phys. Chem Au 2025, 5, 293−301

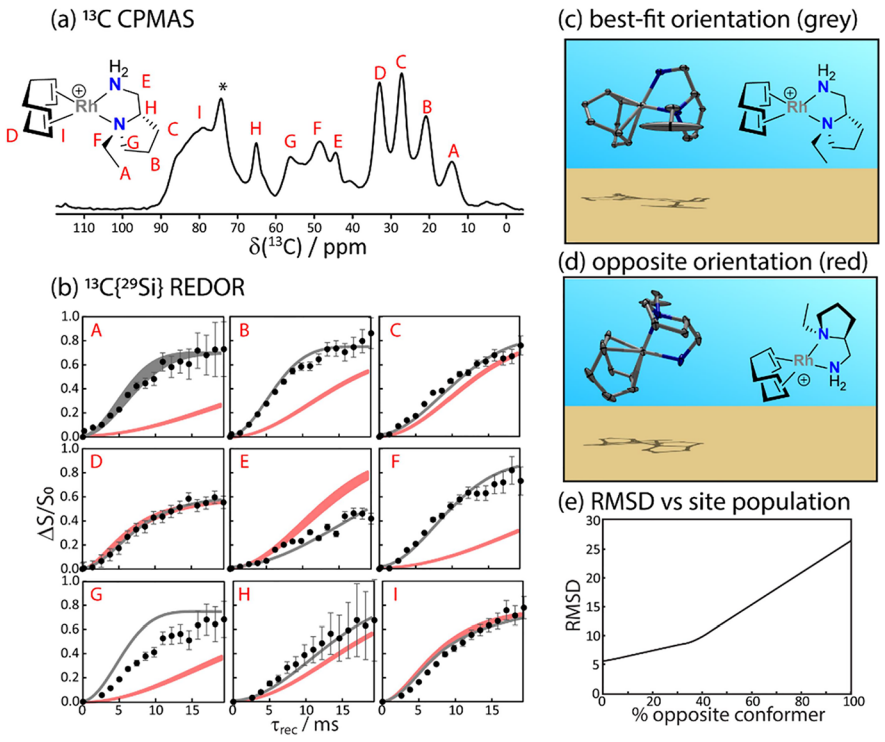

Figure 3. DNP-enhanced ^{13}C CPMAS NMR spectrum of [Rh(cod)(aep)]CF_3SO_3/$^{29}SiO_2$ (a) and results from a $^{13}C\{^{29}Si\}$ REDOR experiment (b). An asterisk denotes a resonance from the 1,1,2,2-tetrachloroethane-d2 solvent. Resonances are assigned according to the structure in (a). The REDOR data is best fitted to the molecular orientation in (c), while an alternate fit to the orientation in (d) is shown in red. Linear combinations of the two orientations do not lead to an improved fit quality (e), suggesting a strong preference for this orientation on the surface.

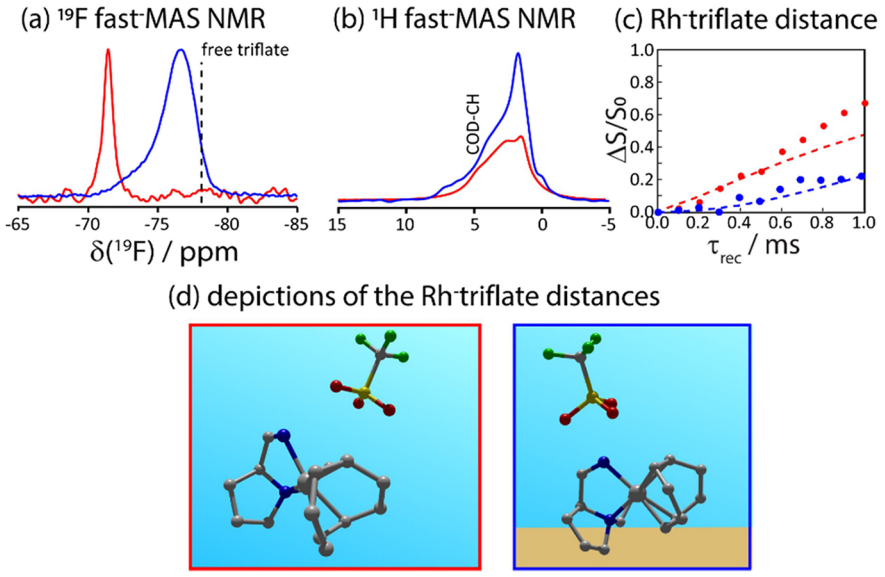

Figure 4. ^{19}F (a) and ^{1}H (b) fast-MAS (40 kHz) NMR spectra of [Rh(cod)(aep)]CF_3SO_3 (red) and [Rh(cod)(aep)]CF_3SO_3/SiO_2 (blue). A dashed line highlights the expected chemical shift of free triflate.[77] (b) $^{1}H\{^{19}F\}$ S-REDOR dephasing data measured for [Rh(cod)(aep)]CF_3SO_3 (red) and [Rh(cod)(aep)]CF_3SO_3/SiO_2 together with the structures used for the fitting (c). (d) The fit for the [Rh(cod)(aep)]CF_3SO_3 uses the crystal structure of the complex.[32]

is notorious for its inability in properly describing noncovalent interactions we also sought to confirm the above-mentioned conclusions using ab initio methods. Cluster models were extracted from the periodic ones and we performed RI-MP2 calculations.[72] These calculations agreed with the aforementioned plane-wave DFT calculations, predicting differences in adsorption energies of 9.0 and 44.4 kJ/mol, corresponding to only 6 and 15% deviations from those calculated using PBE-D3 on the same models (Table S3).

3.3. Role of the Triflate Anion

The above models did not include the triflate counteranion as this would not have allowed for the independent measurement of silica-complex interactions. The clear importance of hydrogen bonding interactions, however, suggests that the

https://doi.org/10.1021/acsphyschemau.5c00007
ACS Phys. Chem Au 2025, 5, 293−301

anion may be required to guide the preferential adsorption of the complex. To probe the interactions between the triflate and the adsorbed [Rh(cod)(aep)]CF_3SO_3 complex, we performed ^{19}F fast-MAS NMR spectroscopy and $^{1}H\{^{19}F\}$ S-REDOR experiments. The results from these measurements are depicted in Figure 4.

The ^{19}F MAS spectra of the crystalline [Rh(cod)(aep)]-CF_3SO_3 complex and the supported variant are shown in Figure 4a. The precursor yields a single resonance at −71.5 ppm, which is shifted to −76.5 ppm in the heterogeneous species. The crystal structure of the precursor contains a sulfonate-NH_2 hydrogen bonding interaction (Figure 4d). Given that free triflate is expected to resonate at approximately −78.1 ppm,[77] the difference in the ^{19}F chemical shifts of the precursor and supported complexes suggests a weaker, albeit still present NH_2-triflate hydrogen bonding interaction.

This conclusion is further supported by the $^{1}H\{^{19}F\}$ S-REDOR experiment (Figure 4c). Due to spectral overlap of the aliphatic signals and the silanols from the surface, only the distance between the cod protons (shoulder in Figure 4b) and the fluorine atoms of the triflate could be probed. We observed slower dephasing in [Rh(cod)(aep)]CF_3SO_3/SiO_2 than [Rh-(cod)(aep)]CF_3SO_3, suggesting again a weaker hydrogen bonding interaction is present in the supported complex. A reasonable SO_3−NH_2 distance of 3 Å can reproduce the observed dephasing when the triflate anion is positioned in a vertical orientation (Figure 4d), although dynamics consistent with the observed change in chemical shift would also explain the difference in the dipolar coupling strength. Importantly, such a hydrogen bonding interaction would be unable to form if the complex adopted an orientation with the NH_2 moiety interacting with silica. This is likely the ultimate factor that forces the complex to adopt the orientation measured in Figure 3.

3.4. Dynamics

Preferred complex adsorption orientations, and how they relate to the reactant-surface interactions[13−17] may only affect reaction outcomes if they are preserved during a reaction. The $^{13}C\{^{29}Si\}$ REDOR experiments used to determine the orientation, however, were performed at a temperature of 100 K, where dynamics are expected to be eliminated. To probe the rigidity of the complex we performed room temperature ^{1}H chemical shift anisotropy (CSA) recoupling experiments using a phase-sensitive γ-encoded sequence[78,60] that enables the measurement of weak anisotropies. The proton CSA was recently shown to be a sensitive probe of molecular motions.[79] The measured recoupled powder patterns are depicted in Figure 5a for the crystalline precursor complex and [Rh(cod)-(aep)]CF_3SO_3/SiO_2 both with and without the addition of solvent (deuterated 1,1,2,2-tetrachloroethane).

We observed a recoupled CSA splitting of 730 Hz, corresponding to an anisotropy (δ_{aniso}) of 4.8 ppm. An identical splitting was measured for the supported species, indicating that the complex is immobile at room temperature. Molecular motions would be expected to dynamically average the anisotropic interaction and thus lead to a reduction in the recoupled splitting. The addition of the solvent did not lead to a shift in the maximum, again suggesting that the complex maintains its preferred orientation when solvent is added, and likely under reaction conditions as well.

Thomas and co-workers observed that the selectivity was increased when the mesopore diameters were reduced due to increased confinement.[32] We repeated the above-mentioned ^{1}H CSA recoupling experiments on [Rh(cod)(aep)]CF_3SO_3/SiO_2 complexes supported onto Davisil-type silica gels with mesopore diameters of 30, 60, and 150 Å, mirroring Thomas' earlier catalysis work, to determine whether rigidity is impacted in less confined environments. We did not observe an increase in millisecond-scale dynamics when the pore diameter was increased, suggesting that the same preferred orientation exists on these supports, however, we did observe a notable reduction in ^{1}H T_1 relaxation time (Figure 5b). Specifically, the relaxation time was reduced from 3.0 to 1.8 and 1.4 s when the pore diameter was increased from 30 to 60 and then 150 Å. This suggests that the complexes supported in the larger pores are more fluctional on a nanosecond time scale which could grant them a higher level of conformational freedom during a reaction.

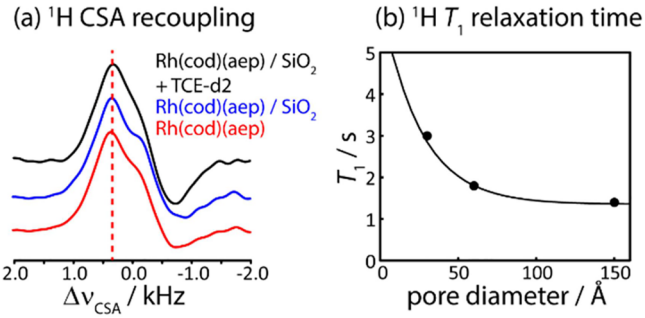

Figure 5. (a) Phase-sensitive ^{1}H CSA recoupled spectra of the cod alkene ^{1}H in [Rh(cod)(aep)]CF_3SO_3 (red), [Rh(cod)(aep)]-CF_3SO_3/SiO_2 (blue), and this same complex wetted with deuterated 1,1,2,2-tetrachloroethane (black). (b) The pore diameter dependence of the ^{1}H T_1 relaxation time of [Rh(cod)(aep)]CF_3SO_3/SiO_2.

4. DISCUSSION

During a methyl benzoylformate hydrogenation reaction, to form methyl mandelate, the incoming reactant can approach the catalyst in four distinct orientations (Figure 6). Specifically, either face of the ketone can be attacked, and the ketone's oxygen can appear either *cis* or *trans* to the aep ligand's NH_2 moiety. Two of the pathways ultimately lead to the formation

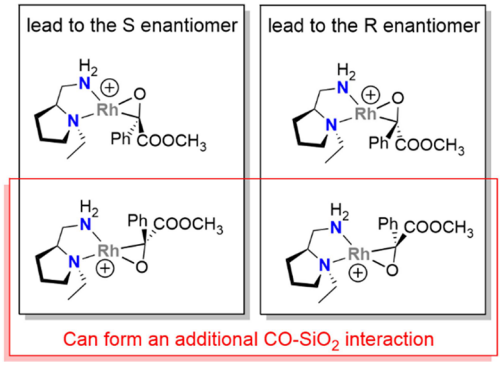

Figure 6. Four competing reaction intermediates lead to the formation of the *S* and *R* enantiomers of methyl mandelate. Owing to the preferred orientation of the complex on silica, and the expected formation of CO-silica noncovalent interactions, the elimination of two competing pathways in the heterogeneous catalyst may be responsible for the enhanced selectivity.

https://doi.org/10.1021/acsphyschemau.5c00007
ACS Phys. Chem Au 2025, 5, 293−301

of the S-methyl mandelate while the other two lead to the *R* enantiomer.

In the heterogeneous case, we observed a strong preference for the complex orienting itself on the surface such that the aep ligands' NH_2 moiety is oriented away from the silica surface, such that it can retain its hydrogen bonding interaction with the triflate anion. NMR experiments aimed at measuring the dynamics of the complex at room temperature and in the presence of solvent have revealed the interaction of the complex with the surface to be quite rigid and as such the expectation is that the aep ligand's orientation would be preserved during a hydrogenation reaction. While in solution, the energetic differences between conformers with their ketone oxygen atoms positioned *cis* or *trans* to the aep's NH_2 moiety may be quite minor, the *trans* conformer enables the formation of CO-HOSi hydrogen bonding interactions. As a result, silica is expected to further bias the orientation of the reactant through surface-reactant intermolecular interactions, much like there is a bias in the orientation of the aep ligand due to triflate-NH_2 hydrogen bonding. Ultimately, these copreferred orientations reduce the number of possible intermediate configurations in half, likely leading to an increase in selectivity. Specifically, the corresponding intermediate which minimizes Ph-aep steric repulsions leads to the experimentally observed *R* enantiomer.

It is nevertheless important to note that while the precatalyst was found to be rigidly bound in this particular orientation, the hydride complex that forms during the reaction may prefer a different conformation. It is also possible that a minor conformer is responsible for the bulk of the catalyst's activity, as has indeed been observed in Rh enantioselective hydrogenation.[80] The modulation of the populations of these sites, whether or not they differ from that observed in the precatalyst, would also be expected to impact selectivity.

Similar observations have been made in other catalytic systems. For instance, Fraile and co-workers studied the cyclopropanation of styrene with ethyl diazoacetate using chiral bis(oxazoline)-copper catalysts electrostatically attached to clay surfaces.[13] Much like that discussed above and in Figure 6, in their system styrene is able to approach the Cu center in four orientations. They observe the predominant formation of the R,R diastereomer in the homogeneous case, due to a minimization of styrene-ligand steric interactions, however, in the heterogeneous system the selectivity is instead reversed and favors the formation of the R,S diastereomer. This result originates from the minimization of styrene-surface steric interactions and the styrene reactant adopting a preferred orientation of approach.

The role that reactant-silica hydrogen bonding interactions play in enantioselective heterogeneous catalysis have also been specifically touched upon by Zhao and co-workers.[16] They studied the organocatalyzed Michael addition of nitromethane onto chalcone using homogeneous and silica-supported heterogeneous 9-amino(9-deoxy)epiquinine and 9-thiourea epiquinine catalysts. They found that the number of possible substrate-surface hydrogen bonds differed for the R and S transition states and that the stabilizing effect of these interactions on the transition states is largely responsible for the observed changes in enantioselectivity. These interactions were further strongly affected by the pore curvature.

Zhao's argument that pore curvature can modulate the number and strength of the reactant-surface interactions is likely of relevance to Thomas' observed increase in enantioselectivity when reducing pore sizes, specifically, by facilitating CO-HOSi interactions.[32] We have also presented further evidence that increases in pore curvature help rigidify the $[Rh(cod)(aep)]CF_3SO_3$ complex. Finding other ways wherein the number of possible transition states is reduced by leveraging preferential adsorption of catalysts and reactants may lead to other discoveries of enhanced selectivity.

5. CONCLUSIONS

Recent advancements in surface-enhanced solid-state NMR spectroscopy enable experimental structural insights that move beyond molecular structure and reveal local configurations and surface orientations. Using such methods, we discovered that $[Rh(cod)(aep)]CF_3SO_3$ adsorbs onto silica in a specific molecular orientation relative to the support, despite the lack of a covalent tether. This preferred orientation was found to be driven by the complex favoring the formation of NH_2-triflate hydrogen bonds. Owing to an expected similar preference for the reactant to orient itself to maximize its interactions with the support, the preferential adsorption of the catalyst is expected to reduce the number of possible intermediates from four to two, leading to the experimentally observed increase in enantioselectivity. We believe these ideas of preferential molecular orientations in heterogeneous catalysis reactions to be universal and a general approach whereby one can enhance or reverse the selectivity of a catalyst.

■ ASSOCIATED CONTENT

Supporting Information

The Supporting Information is available free of charge at https://pubs.acs.org/doi/10.1021/acsphyschemau.5c00007.

Liquid-state NMR data, all REDOR data, NMR-derived structures, DFT-optimized structures and their energies, and INTERFACES input files used to analyze the NMR data (PDF)

Data (ZIP)

■ AUTHOR INFORMATION

Corresponding Author

Frédéric A. Perras − *Division of Chemical and Biological Sciences, Ames National Laboratory, Ames, Iowa 50011, United States; Department of Chemistry, Iowa State University, Ames, Iowa 50011, United States;* orcid.org/0000-0002-2662-5119; Email: fperras@ameslab.gov

Authors

Guillaume P. Laurent − *Division of Chemical and Biological Sciences, Ames National Laboratory, Ames, Iowa 50011, United States; CNRS, Laboratoire de Chimie de la Matière Condensée de Paris, LCMCP, Sorbonne Université, F-75005 Paris, France;* orcid.org/0000-0002-8127-5326

Samuel L. Leonard − *Department of Chemistry, Iowa State University, Ames, Iowa 50011, United States;* orcid.org/0000-0001-5535-8016

Mita Halder − *Division of Chemical and Biological Sciences, Ames National Laboratory, Ames, Iowa 50011, United States;* orcid.org/0000-0002-2221-4259

Damien B. Culver − *Division of Chemical and Biological Sciences, Ames National Laboratory, Ames, Iowa 50011, United States;* orcid.org/0000-0001-8294-6059

Peng Xu − *Division of Chemical and Biological Sciences, Ames National Laboratory, Ames, Iowa 50011, United States; Department of Chemistry, Iowa State University, Ames, Iowa 50011, United States;* orcid.org/0000-0002-7762-8934

Mark S. Gordon − *Division of Chemical and Biological Sciences, Ames National Laboratory, Ames, Iowa 50011, United States; Department of Chemistry, Iowa State University, Ames, Iowa 50011, United States*

Complete contact information is available at: https://pubs.acs.org/10.1021/acsphyschemau.5c00007

Author Contributions

NMR experiments and material preparation were carried out by G.L. and F.P. and analyzed by both authors. Solution-phase NMR and infrared spectroscopy was performed by M.H. and D.C. Density functional theory calculations were carried out by F.P. Møller−Plesset perturbation theory calculations were carried out by S.L. under the direction of P.X. and M.G. All authors contributed to the writing of the article.

Notes

The authors declare no competing financial interest.

■ ACKNOWLEDGMENTS

This work was supported by the U.S. Department of Energy (DOE), Office of Basic Energy Sciences, Division of Chemical Sciences, Geosciences, and Biosciences through a DOE Early Career Project. Synthesis work was supported as a part of the Ames National laboratory catalysis project. RI-MP2 calculations were supported by the Ames National Laboratory Computational and Theoretical Chemistry (CTC) project. Ames National Laboratory is operated for the DOE by Iowa State University under Contract No. DE-AC02-07CH11358.

■ REFERENCES

(1) Thomas, J. M.; Raja, R. Exploiting Nanospace for Asymmetric Catalysis: Confinement of Immobilized, Single-Site Chiral Catalysts Enhances Enantioselectivity. *Acc. Chem. Res.* **2008**, *41* (6), 708−720.

(2) Fraile, J. M.; García, J. I.; Herrerías, C. I.; Mayoral, J. A.; Pires, E. Enantioselective catalysis with chiral complexes immobilized on nanostructured supports. *Chem. Soc. Rev.* **2009**, *38* (3), 695−706.

(3) Motokura, K.; Ding, S.; Usui, K.; Kong, Y. Enhanced Catalysis Based on the Surface Environment of the Silica-Supported Metal Complex. *ACS Catal.* **2021**, *11* (19), 11985−12018.

(4) Zaera, F. Designing Sites in Heterogeneous Catalysis: Are We Reaching Selectivities Competitive With Those of Homogeneous Catalysts? *Chem. Rev.* **2022**, *122* (9), 8594−8757.

(5) Chien, J. C. W.; Vizzini, J. C.; Kaminsky, W. Difference in stereoselective polymerization of 4-methyl-1-hexene by homogeneous and heterogeneous Ziegler-Natta catalysts. *Makromol. Chem. Rapid Commun.* **1992**, *13* (11), 479−484.

(6) Brintzinger, H. H.; Fischer, D.; Mülhaupt, R.; Rieger, B.; Waymouth, R. M. Stereospecific Olefin Polymerization with Chiral Metallocene Catalysts. *Angew. Chem., Int. Ed.* **1995**, *34* (11), 1143−1170.

(7) Coates, G. W. Polymerization catalysis at the millennium: frontiers in stereoselective, metal-catalyzed polymerization. *J. Chem. Soc., Dalton Trans.* **2002**, *4*, 467−475.

(8) Bahri-Laleh, N.; Hanifpour, A.; Mirmohammadi, S. A.; Poater, A.; Nekoomanesh-Haghighi, M.; Talarico, G.; Cavallo, L. Computational modeling of heterogeneous Ziegler-Natta catalysts for olefins polymerization. *Prog. Polym. Sci.* **2018**, *84*, 89−114.

(9) Zhang, J.; Mason, A. H.; Wang, Y.; Motta, A.; Kobayashi, T.; Pruski, M.; Gao, Y.; Marks, T. J. Beyond the Active Site. Cp*ZrMe3/Sulfated Alumina-Catalyzed Olefin Polymerization Tacticity via Catalyst···Surface Ion-Pairing. *ChemCatChem.* **2021**, *13* (11), 2564−2569.

(10) Ajellal, N.; Durieux, G.; Delevoye, L.; Tricot, G.; Dujardin, C.; Thomas, C. M.; Gauvin, R. M. Polymerization of racemic β-butyrolactone using supported catalysts: a simple access to isotactic polymers. *Chem. Commun.* **2010**, *46* (7), 1032−1034.

(11) Gauvin, R. M.; Mortreux, A. Silica-supported lanthanide silylamides for methyl methacrylate polymerisation: controlled grafting induces controlled reactivity. *Chem. Commun.* **2005**, *9*, 1146−1148.

(12) Fernández, A. I.; Fraile, J. M.; García, J. I.; Herrerías, C. I.; Mayoral, J. A.; Salvatella, L. Reversal of enantioselectivity by change of solvent with clay-immobilized bis(oxazoline)−copper catalysts. *Catal. Commun.* **2001**, *2* (5), 165−170.

(13) Fraile, J. M.; García, J. I.; Harmer, M. A.; Herrerías, C. I.; Mayoral, J. A.; Reiser, O.; Werner, H. Immobilisation of bis-(oxazoline)−copper complexes on clays and nanocomposites. Influence of different parameters on activity and selectivity. *J. Mater. Chem.* **2002**, *12* (11), 3290−3295.

(14) Castillo, M. R.; Fousse, L.; Fraile, J. M.; García, J. I.; Mayoral, J. A. Supported Ionic-Liquid Films (SILF) as Two-Dimensional Nanoreactors for Enantioselective Reactions: Surface-Mediated Selectivity Modulation (SMSM). *Chem.—Eur. J.* **2007**, *13* (1), 287−291.

(15) Hong, J.; Zaera, F. Interference of the Surface of the Solid on the Performance of Tethered Molecular Catalysts. *J. Am. Chem. Soc.* **2012**, *134* (31), 13056−13065.

(16) Zhao, L.; Li, Y.; Yu, P.; Han, X.; He, J. Exploration of Dependence of Organo-Catalyzed Enantioselective Michael Addition on the Pore Size of Mesoporous Host. *ACS Catal.* **2012**, *2* (6), 1118−1126.

(17) Shu, X.-Z.; Nguyen, S. C.; He, Y.; Oba, F.; Zhang, Q.; Canlas, C.; Somorjai, G. A.; Alivisatos, A. P.; Toste, F. D. Silica-Supported Cationic Gold(I) Complexes as Heterogeneous Catalysts for Regio- and Enantioselective Lactonization Reactions. *J. Am. Chem. Soc.* **2015**, *137* (22), 7083−7086.

(18) Johnson, B. F. G.; Raynor, S. A.; Shephard, D. S.; Mashmeyer, T.; Thomas, J. M.; Sankar, G.; Bromley, S.; Oldroyd, R.; Gladden, L.; Mantle, M. D. Superior performance of a chiral catalyst confined within mesoporous silica. *Chem. Commun.* **1999**, *13*, 1167−1168.

(19) Piaggio, P.; McMorn, P.; Murphy, D.; Bethell, D.; Page, P. C. B.; Hancock, F. E.; Sly, C.; Kerton, O. J.; Hutchings, G. J. Enantioselective epoxidation of (Z)-stilbene using a chiral Mn-(III)−salen complex: effect of immobilisation on MCM-41 on product selectivity. *J. Chem. Soc., Perkin Trans.* **2000**, *2* (10), 2008−2015.

(20) Xiang, S.; Zhang, Y.; Xin, Q.; Li, C. Enantioselective epoxidation of olefins catalyzed by Mn (salen)/MCM-41 synthesized with a new anchoring method. *Chem. Commun.* **2002**, *22*, 2696−2697.

(21) Jones, M. D.; Raja, R.; Thomas, J. M.; Johnson, B. F. G.; Lewis, D. W.; Rouzaud, J.; Harris, K. D. M. Enhancing the Enantioselectivity of Novel Homogeneous Organometallic Hydrogenation Catalysts. *Angew. Chem., Int. Ed.* **2003**, *42* (36), 4326−4331.

(22) Hultman, H. M.; de Lang, M.; Arends, I. W. C. E.; Hanefeld, U.; Sheldon, R. A.; Maschmeyer, T. Chiral catalysts confined in porous hosts: 2. Catalysis. *J. Catal.* **2003**, *217* (2), 275−283.

(23) Zhang, H.; Xiang, S.; Li, C. Enantioselective epoxidation of unfunctionalised olefins catalyzed by Mn(salen) complexes immobilized in porous materials via phenyl sulfonic group. *Chem. Commun.* **2005**, *9*, 1209−1211.

(24) Fraile, J. M.; García, J. I.; Mayoral, J. A.; Roldán, M. Simple and Efficient Heterogeneous Copper Catalysts for Enantioselective C−H Carbene Insertion. *Org. Lett.* **2007**, *9* (4), 731−733.

(25) Fabra, M. J.; Fraile, J. M.; Herrerías, C. I.; Lahoz, F. J.; Mayoral, J. A.; Pérez, I. Surface-enhanced stereoselectivity in Mukaiyama aldol reactions catalyzed by clay-supported bis(oxazoline)−copper complexes. *Chem. Commun.* **2008**, *42*, 5402−5404.

(26) Kawamorita, S.; Ohmiya, H.; Hara, K.; Fukuoka, A.; Sawamura, M. Directed Ortho Borylation of Functionalized Arenes Catalyzed by

a Silica-Supported Compact Phosphine−Iridium System. *J. Am. Chem. Soc.* **2009**, *131* (14), 5058−5059.
(27) Yang, Y.; Rioux, R. M. Highly regio- and stereoselective hydrothiolation of acetylenes with thiols catalyzed by a well-defined supported Rh complex. *Chem. Commun.* **2011**, *47* (23), 6557−6559.
(28) Xia, D.; Cheng, T.; Xiao, W.; Liu, K.; Wang, Z.; Liu, G.; Li, H.; Wang, W. Imidazolium-Based Organic−Inorganic Hybrid Silica as a Functional Platform Dramatically Boosts Chiral Organometallics Performance in Asymmetric Catalysis. *ChemCatChem.* **2013**, *5* (7), 1784−1789.
(29) Fernandes, C. I.; Saraiva, M. S.; Nunes, T. G.; Vas, P. D.; Nunes, C. D. Highly enantioselective olefin epoxidation controlled by helical confined environments. *J. Catal.* **2014**, *309*, 21−32.
(30) Yang, Y.; Chang, J. W.; Rioux, R. M. Structural elucidation of supported Rh complexes derived from $RhCl(PPh_3)_3$ immobilized on surface-functionalized SBA-15 and their catalytic performance for C-heteroatom (S, O) bond formation. *J. Catal.* **2018**, *365*, 43−54.
(31) Rouzaud, J.; Jones, M. D.; Raja, R.; Johnson, B. F. G.; Thomas, J. M.; Duer, M. J. Potent new heterogeneous asymmetric catalysts. *Helv. Chim. Acta* **2003**, *86* (5), 1753−1759.
(32) Raja, R.; Thomas, J. M.; Jones, M. D.; Johnson, B. F. G.; Vaughan, D. E. W. Constraining Asymmetric Organometallic Catalysts within Mesoporous Supports Boosts Their Enantioselectivity. *J. Am. Chem. Soc.* **2003**, *125* (49), 14982−14983.
(33) Gerstberger, G.; Anwander, R. Screening of rare earth metal grafted MCM-41 silica for asymmetric catalysis. *Microporous Mesoporous Mater.* **2001**, *44*−*45*, 303−310.
(34) Baleizão, C.; Gigante, B.; Garcia, H.; Corma, A. Chiral vanadyl Schiff base complex anchored on silicas as solid enantioselective catalysts for formation of cyanohydrins: optimization of the asymmetric induction by support modification. *J. Catal.* **2003**, *215* (2), 199−207.
(35) O'Leary, P.; Krosveld, N. P.; De Jong, K. P.; van Koten, G.; Gebbink, R. J. M. K. Facile and rapid immobilization of copper(II) bis(oxazoline) catalysts on silica: application to Diels−Alder reactions, recycling, and unexpected effects on enantioselectivity. *Tetrahedron Lett.* **2004**, *45* (16), 3177−3180.
(36) Wang, H.; Liu, X.; Xia, H.; Liu, P.; Gao, J.; Ying, P.; Xiao, J.; Li, C. Asymmetric Diels−Alder reactions with hydrogen bonding heterogeneous catalysts and mechanistic studies on the reversal of enantioselectivity. *Tetrahedron* **2006**, *62* (5), 1025−1032.
(37) Zhang, H.; Zhang, Y.; Li, C. Enantioselective epoxidation of unfunctionalized olefins catalyzed by the Mn(salen) catalysts immobilized in the nanopores of mesoporous materials. *J. Catal.* **2006**, *238* (2), 369−381.
(38) Tanaka, S.; Tada, M.; Iwasawa, Y. Enantioselectivity promotion by achiral surface functionalization on SiO_2-supported Cu-bis-(oxazoline) catalysts for asymmetric Diels−Alder reactions. *J. Catal.* **2007**, *245* (1), 173−183.
(39) Gill, C. S.; Venkatasubbaiah, K.; Jones, C. W. Recyclable Polymer- and Silica-Supported Ruthenium(II)-Salen Bis-Pyridine Catalysts for the Asymmetric Cyclopropanation of Olefins. *Adv. Synth. Catal.* **2009**, *351* (9), 1344−1354.
(40) Himiyama, T.; Waki, M.; Maegawa, Y.; Inagaki, S. Cooperative Catalysis of an Alcohol Dehydrogenase and Rhodium-Modified Periodic Mesoporous Organosilica. *Angew. Chem., Int. Ed.* **2019**, *58* (27), 9150−9154.
(41) Maly, T.; Debelouchina, G. T.; Bajaj, V. S.; Hu, K.-N.; Joo, C.-G.; Mak-Jurkauskas, M. L.; Sirigiri, J. R.; van der Wel, P. C. A.; Herzfeld, J.; Temkin, R. J.; Griffin, R. G. Dynamic nuclear polarization at high magnetic fields. *J. Chem. Phys.* **2008**, *128* (5), No. 052211.
(42) Lesage, A.; Lelli, M.; Gajan, D.; Caporini, M. A.; Vitzthum, V.; Miéville, P.; Alauzun, J.; Roussey, A.; Thieuleux, C.; Mehdi, A.; Bodenhausen, G.; Copéret, C.; Emsley, L. Surface Enhanced NMR Spectroscopy by Dynamic Nuclear Polarization. *J. Am. Chem. Soc.* **2010**, *132* (44), 15459−15461.
(43) Kobayashi, T.; Perras, F. A.; Slowing, I. I.; Sadow, A. D.; Pruski, M. Dynamic Nuclear Polarization Solid-State NMR in Heterogeneous Catalysis Research. *ACS Catal.* **2015**, *5*, 7055−7062.
(44) Perras, F. A.; Padmos, J. D.; Johnson, R. L.; Wang, L.-L.; Schwartz, T. J.; Kobayashi, T.; Horton, J. H.; Dumesic, J. A.; Shanks, B. H.; Johnson, D. D.; Pruski, M. Characterizing Substrate−Surface Interactions on Alumina-Supported Metal Catalysts by Dynamic Nuclear Polarization-Enhanced Double-Resonance NMR Spectroscopy. *J. Am. Chem. Soc.* **2017**, *139* (7), 2702−2709.
(45) Perras, F. A.; Paterson, A. L.; Syed, Z. H.; Kropf, A. J.; Kaphan, D. M.; Delferro, M.; Pruski, M. Revealing the Configuration and Conformation of Surface Organometallic Catalysts with DNP-Enhanced NMR. *J. Phys. Chem. C* **2021**, *125* (24), 13433−13442.
(46) Jabbour, R.; Renom-Carrasco, M.; Chan, K. W.; Völker, L.; Berruyer, P.; Wang, Z.; Widdifield, C. M.; Lelli, M.; Gajan, D.; Copéret, C.; Thieuleux, C.; Lesage, A. Multiple Surface Site Three-Dimensional Structure Determination of a Supported Molecular Catalyst. *J. Am. Chem. Soc.* **2022**, *144* (23), 10270−10281.
(47) Perras, F. A.; Arroyave, A.; Southern, S. A.; Lamb, J. V.; Li, Y.; LaPointe, A.; Delferro, M. Double-resonance ^{17}O NMR experiments reveal unique configurational information for surface organometallic complexes. *Chem. Commun.* **2023**, *59* (31), 4604−4607.
(48) Perras, F. A.; Culver, D. B. On the use of NMR distance measurements for assessing surface site homogeneity. *Dalton Trans.* **2023**, *52* (48), 18502−18512.
(49) Southern, S. A.; Li, Y.; Liu, D.-J.; Sadow, A. D.; Qi, L.; Perras, F. A. Enhanced Activity from Coordinatively Unsaturated and Dynamic Zeolite-Bound Organoscandium Species. *ACS Catal.* **2024**, *14* (12), 9440−9451.
(50) Berruyer, P.; Lelli, M.; Conley, M. P.; Silverio, D. L.; Widdifield, C. M.; Siddiqi, G.; Gajan, D.; Lesage, A.; Copéret, C.; Emsley, L. Three-Dimensional Structure Determination of Surface Sites. *J. Am. Chem. Soc.* **2017**, *139* (2), 849−855.
(51) Perras, F. A.; Kanbur, U.; Paterson, A. L.; Chatterjee, P.; Slowing, I. I.; Sadow, A. D. Determining the Three-Dimensional Structures of Silica-Supported Metal Complexes from the Ground Up. *Inorg. Chem.* **2022**, *61* (2), 1067−1078.
(52) Cunningham, J.; Perras, F. A. INTERFACES. A program for determining the 3D structures of surfaces sites using NMR data. *J. Magn. Reson. Open* **2022**, *12*−*13*, No. 100066.
(53) Kobayashi, T.; Singappuli-Arachchige, D.; Wang, Z.; Slowing, I. I.; Pruski, M. Spatial distribution of organic functional groups supported on mesoporous silica nanoparticles: a study by conventional and DNP-enhanced ^{29}Si solid-state NMR. *Phys. Chem. Chem. Phys.* **2017**, *19* (3), 1781−1789.
(54) Kobayashi, T.; Slowing, I.; Pruski, M. Measuring Long-Range $^{13}C-^{13}C$ Correlations on a Surface under Natural Abundance Using Dynamic Nuclear Polarization-Enhanced Solid-State Nuclear Magnetic Resonance. *J. Phys. Chem. C* **2017**, *121* (44), 24687−24691.
(55) Kobayashi, T.; Singappuli-Arachchige, D.; Slowing, I. I.; Pruski, M. Spatial distribution of organic functional groups supported on mesoporous silica nanoparticles (2): a study by ^{1}H triple-quantum fast-MAS solid-state NMR. *Phys. Chem. Chem. Phys.* **2018**, *20* (34), 22203−22209.
(56) Kobayashi, T.; Pruski, M. Spatial Distribution of Silica-Bound Catalytic Organic Functional Groups Can Now Be Revealed by Conventional and DNP-Enhanced Solid-State NMR Methods. *ACS Catal.* **2019**, *9* (8), 7238−7249.
(57) Gao, J.; Dorn, R. W.; Laurent, G. P.; Perras, F. A.; Rossini, A. J.; Conley, M. P. A Heterogeneous Palladium Catalyst for the Polymerization of Olefins Prepared by Halide Abstraction Using Surface R_3Si^+ Species. *Angew. Chem., Int. Ed.* **2022**, *61* (20), No. e202117279.
(58) Kobayashi, T.; Liu, D.-J.; Perras, F. A. Spatial arrangement of dynamic surface species from solid-state NMR and machine learning-accelerated MD simulations. *Chem. Commun.* **2022**, *58* (100), 13939−13942.
(59) Lee, D.; Wolska-Pietkiewicz, M.; Badoni, S.; Grala, A.; Lewiński, J.; De Paëpe, G. Disclosing Interfaces of ZnO Nanocrystals Using Dynamic Nuclear Polarization: Sol-Gel versus Organometallic Approach. *Angew. Chem., Int. Ed.* **2019**, *58* (48), 17163−17168.

(60) Perras, F. A.; Paterson, A. L.; Kobayashi, T. Phase-sensitive gamma-encoded recoupling of heteronuclear dipolar interactions and ^{1}H chemical shift anisotropy. *Solid State Nucl. Magn. Reson.* **2021**, *111*, No. 101712.
(61) Gullion, T.; Schaefer, J. Rotational-echo double-resonance NMR. *J. Magn. Reson.* **1989**, *81* (1), 196−200.
(62) Chen, L.; Wang, Q.; Hu, B.; Lafon, O.; Trébosc, J.; Deng, F.; Amoureux, J.-P. Measurement of hetero-nuclear distances using a symmetry-based pulse sequence in solid-state NMR. *Phys. Chem. Chem. Phys.* **2010**, *12* (32), 9395−9405.
(63) Brinkmann, A.; Kentgens, A. P. M. Proton-selective ^{17}O-^{1}H distance measurements in fast magic-angle-spinning solid-state NMR spectroscopy for the determination of hydrogen bond lengths. *J. Am. Chem. Soc.* **2006**, *128* (46), 14758−14759.
(64) Zagdoun, A.; Casano, G.; Ouari, O.; Schwarzwälder, M.; Rossini, A. J.; Aussenac, F.; Yulikov, M.; Jeschke, G.; Copéret, C.; Lesage, A.; Tordo, P.; Emsley, L. Large molecular weight nitroxide biradicals providing efficient dynamic nuclear polarization at temperatures up to 200 K. *J. Am. Chem. Soc.* **2013**, *135* (34), 12790−12797.
(65) Kobayashi, T.; Perras, F. A.; Chaudhary, U.; Slowing, I. I.; Huang, W.; Sadow, A. D.; Pruski, M. Improved strategies for DNP-enhanced 2D ^{1}H-X heteronuclear correlation spectroscopy of surfaces. *Solid State Nucl. Magn. Reson.* **2017**, *87*, 38−44.
(66) Zagdoun, A.; Rossini, A. J.; Gajan, D.; Bourdolle, A.; Ouari, O.; Rosay, M.; Maas, W. E.; Tordo, P.; Lelli, M.; Emsley, L.; Lesage, A.; Copéret, C. Non-aqueous solvents for DNP surface enhanced NMR spectroscopy. *Chem. Commun.* **2012**, *48* (5), 654.
(67) Ugliengo, P.; Sodupe, M.; Musso, F.; Bush, I. J.; Orlando, R.; Dovesi, R. Realistic Models of Hydroxylated Amorphous Silica Surfaces and MCM-41 Mesoporous Material Simulated by Large-scale Periodic B3LYP Calculations. *Adv. Mater.* **2008**, *20* (23), 4579−4583.
(68) Signorile, M.; Salvini, C.; Zamirri, L.; Bonino, F.; Martra, G.; Sodupe, M.; Ugliengo, P. Formamide Adsorption at the Amorphous Silica Surface: A Combined Experimental and Computational Approach. *Life* **2018**, *8* (4), 42.
(69) Giannozzi, P.; Baroni, S.; Bonini, N.; Calandra, M.; Car, R.; Cavazzoni, C.; Ceresoli, D.; Chiarotti, G. L.; Cococcioni, M.; Dabo, I.; Corso, A. D.; de Gironcoli, S.; Fabris, S.; Fratesi, G.; Gebauer, R.; Gerstmann, U.; Gougoussis, C.; Kokalj, A.; Lazzeri, M.; Martin-Samos, L.; Marzari, N.; Mauri, F.; Mazzarello, R.; Paolini, S.; Pasquarello, A.; Paulatto, L.; Sbraccia, C.; Scandolo, S.; Sclauzero, G.; Seitsonen, A. P.; Smogunov, A.; Umari, P.; Wentzcovitch, R. M. QUANTUM ESPRESSO: A Modular and Open-Source Software Project for Quantum Simulations of Materials. *J. Phys.: Condens. Matter* **2009**, *21* (39), No. 395502.
(70) Perdew, J. P.; Burke, K.; Ernzerhof, M. Generalized Gradient Approximation Made Simple. *Phys. Rev. Lett.* **1996**, *77*, 3865−3868.
(71) Grimme, S.; Antony, J.; Ehrlich, S.; Krieg, H. A consistent and accurate ab initio parametrization of density functional dispersion correction (DFT-D) for the 94 elements H-Pu. *J. Chem. Phys.* **2010**, *132* (15), 154104.
(72) Pham, B. Q.; Gordon, M. S. Compressing the Four-Index Two-Electron Repulsion Integral Matrix using the Resolution-of-the-Identity Approximation Combined with the Rank Factorization Approximation. *J. Chem. Theor.Comput.* **2019**, *15* (4), 2254−2264.
(73) te Velde, G.; Bickelhaupt, F. M.; Baerends, E. J.; Fonseca Guerra, C.; van Gisbergen, S. J. A.; Snijders, J. G.; Ziegler, T. Chemistry with ADF. *J. Comput. Chem.* **2001**, *22* (9), 931−967.
(74) Gordon, M. S.; Schmidt, M. W. Chapter 41 - Advances in electronic structure theory: GAMESS a decade later. In *Theory and Applications of Computational Chemistry*; Dykstra, C. E.; Frenking, G.; Kim, K. S.; Scuseria, G. E., Eds.; Elsevier, 2005.
(75) Barca, G. M. J.; Bertoni, C.; Carrington, L.; Datta, D.; De Silva, N.; Deustua, J. E.; Fedorov, D. G.; Gour, J. R.; Gunina, A. O.; Guidez, E.; et al. Recent developments in the general atomic and molecular electronic structure system. *J. Chem. Phys.* **2020**, *152* (15), 154102.
(76) Zahariev, F.; Xu, P.; Westheimer, B. M.; Webb, S.; Vallejo, J. G.; Tiwari, A.; Sundriyal, V.; Sosonkina, M.; Shen, J.; Schoendorff, G.; et al. The General Atomic and Molecular Electronic Structure System (GAMESS): Novel Methods on Novel Architectures. *J. Chem. Theory Comput.* **2023**, *19* (20), 7031−7055.
(77) Zuccaccia, D.; Pirondini, L.; Pinnalli, R.; Dalcanale, E.; Macchioni, A. Dynamic and Structural NMR Studies of Cavitand-Based Coordination Cages. *J. Am. Chem. Soc.* **2005**, *127* (19), 7025−7032.
(78) Pandey, M. K.; Malon, M.; Ramamoorthy, A.; Nishiyama, Y. Composite-180° pulse-based symmetry sequences to recouple proton chemical shift anisotropy tensors under ultrafast MAS solid-state NMR spectroscopy. *J. Magn. Reson.* **2015**, *250*, 45−54.
(79) Southern, S. A.; Liu, D.-J.; Chatterjee, P.; Li, Y.; Perras, F. A. ^{1}H chemical shift anisotropy: a high sensitivity solid-state NMR dynamics probe for surface studies? *Phys. Chem. Chem. Phys.* **2023**, *25* (7), 5348−5360.
(80) Landis, C. R.; Halpern, J. Asymmetric hydrogenation of methyl (Z)-.alpha. acetamidocinnamate catalyzed by [1,2-bis(phenyl-o-anisoyl)phosphino)ethane]rhodium(I): kinetics, mechanism and origin of enantioselection. *J. Am. Chem. Soc.* **1987**, *109* (6), 1746−1754.

https://doi.org/10.1021/acsphyschemau.5c00007
ACS Phys. Chem Au 2025, 5, 293−301